Cell

The RNA Helicase Mtr4p Modulates Polyadenylation in the TRAMP Complex

Huijue Jia,[1] Xuying Wang,[2] Fei Liu,[1] Ulf-Peter Guenther,[1] Sukanya Srinivasan,[1] James T. Anderson,[2] and Eckhard Jankowsky[1,*]
[1]Center for RNA Molecular Biology & Department of Biochemistry, School of Medicine, Case Western Reserve University, Cleveland, OH 44106, USA
[2]Department of Biological Sciences, Marquette University, Milwaukee, WI 53201, USA
*Correspondence: exj13@case.edu
DOI 10.1016/j.cell.2011.05.010

SUMMARY

Many steps in nuclear RNA processing, surveillance, and degradation require TRAMP, a complex containing the poly(A) polymerase Trf4p, the Zn-knuckle protein Air2p, and the RNA helicase Mtr4p. TRAMP polyadenylates RNAs designated for decay or trimming by the nuclear exosome. It has been unclear how polyadenylation by TRAMP differs from polyadenylation by conventional poly(A) polymerase, which produces poly(A) tails that stabilize RNAs. Using reconstituted *S. cerevisiae* TRAMP, we show that TRAMP inherently suppresses poly(A) addition after only 3–4 adenosines. This poly(A) tail length restriction is controlled by Mtr4p. The helicase detects the number of 3′-terminal adenosines and, over several adenylation steps, elicits precisely tuned adjustments of ATP affinities and rate constants for adenylation and TRAMP dissociation. Our data establish Mtr4p as a critical regulator of polyadenylation by TRAMP and reveal that an RNA helicase can control the activity of another enzyme in a highly complex fashion and in response to features in RNA.

INTRODUCTION

The *Trf*4/*Air*2/*M*tr4 *p*olyadenylation (TRAMP) complex is critical for many RNA-processing events in the cell nucleus (Anderson and Wang, 2009; Houseley and Tollervey, 2009). In addition, TRAMP is essential for the nuclear turnover of incorrectly processed RNAs (Houseley and Tollervey, 2008; Kadaba et al., 2004). TRAMP consists of three subunits that are highly conserved in eukaryotes; a noncanonical poly(A) polymerase (Trf4p or Trf5p in *S. cerevisiae*), a Zn-knuckle protein (Air2p or Air1p), and an RNA helicase (Mtr4p/Dob1p) (Jensen and Moore, 2005; LaCava et al., 2005; Vanácová et al., 2005; Wyers et al., 2005). TRAMP polyadenylates RNAs designated for further processing or complete 3′ to 5′ degradation by the nuclear exosome (Bonneau et al., 2009; Liu et al., 2006; Lykke-Andersen et al., 2009). TRAMP and the nuclear exosome have also been linked to chromatin maintenance, remodeling, transcriptional regulation by noncoding RNAs, and DNA repair (Egecioglu et al., 2006; Houseley and Tollervey, 2008; San Paolo et al., 2009). In these processes, TRAMP and the nuclear exosome are thought to function analogously to their roles in RNA processing and degradation; the nuclear exosome degrades presumably nascent RNAs that are polyadenylated by TRAMP (Houseley and Tollervey, 2008).

Polyadenylation by TRAMP is distinct from mRNA polyadenylation by canonical poly(A) polymerases (PAP) (Anderson and Wang, 2009). Polyadenylation by PAP stabilizes mRNAs and requires specific sequence signals in the RNAs (Keller, 1995; Scorilas, 2002; Wilusz and Spector, 2010). In contrast, polyadenylation by TRAMP designates RNAs for degradation or processing, and TRAMP polyadenylates a large cross-section of diverse RNAs without shared sequence or apparent secondary structure and without common associated proteins (Anderson and Wang, 2009; Houseley and Tollervey, 2008).

Given the opposite goals of the two polyadenylation processes, RNAs polyadenylated by PAP must be distinct from RNAs polyadenylated by TRAMP. Indeed, recent data show a marked difference in the length of the respective poly(A) tails in vivo. Whereas PAP typically appends several dozen to hundreds of adenosines (Keller, 1995), RNAs adenylated by TRAMP contain significantly shorter poly(A) tails (Grzechnik and Kufel, 2008; Keller, 1995; Lebreton et al., 2008). Recent data indicate that the distribution of RNAs polyadenylated by TRAMP shows a clear peak at 4 to 5 added nucleotides (Wlotzka et al., 2011).

How polyadenylation by TRAMP is controlled is unknown and not apparent from the current model of TRAMP function. In this model, Trf4p acts as the principal poly(A) polymerase, assisted by Air2p, which is required for Trf4p activity in vitro (Anderson and Wang, 2009; Houseley and Tollervey, 2008). The Ski2-like RNA helicase Mtr4p is thought to subsequently unwind RNA duplexes with 3′ to 5′ polarity (Wang et al., 2008). Mtr4p (Dob1p) was the first factor implicated in aiding RNA degradation by the exosome (de la Cruz et al., 1998). It is thought that unwinding activity of Mtr4p, shown for the recombinant protein, stimulates RNA degradation (Bernstein et al., 2008; Wang et al., 2008; Anderson and Wang, 2009; Houseley and Tollervey, 2008). This basic model of TRAMP function has been instructive in assigning enzymatic roles to the components. However, the model

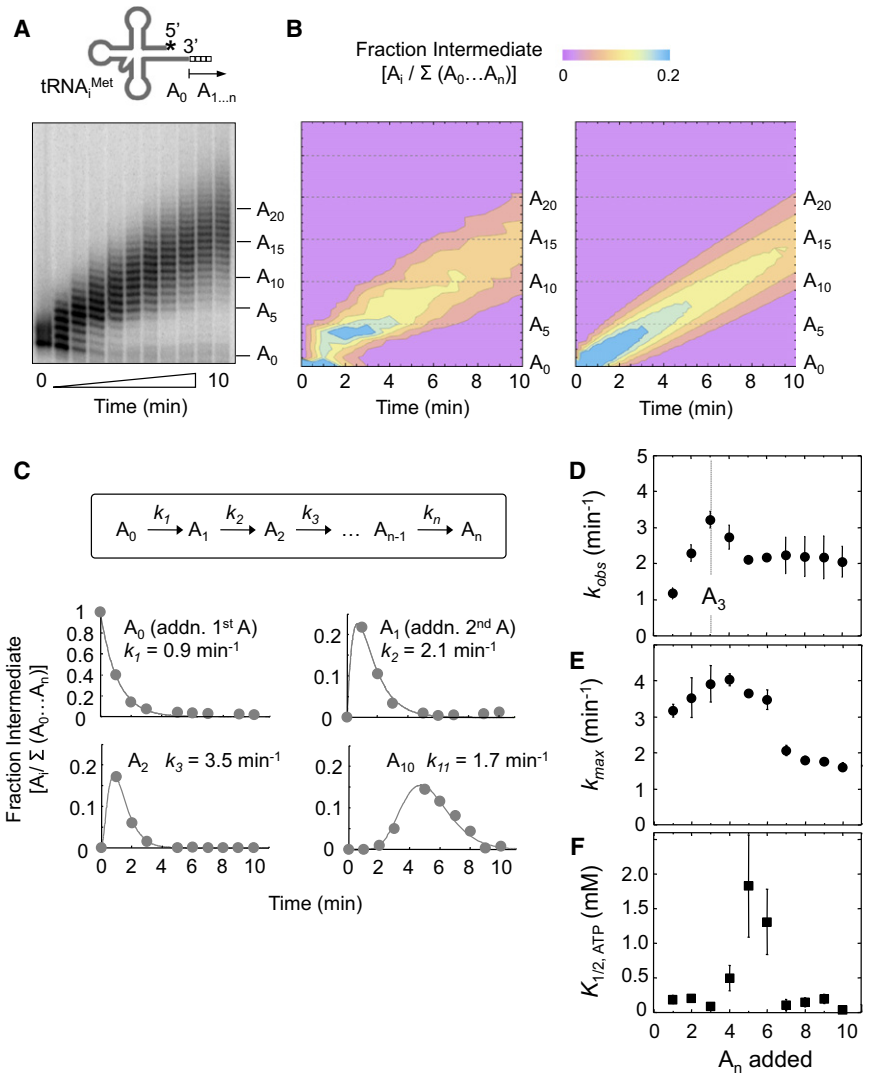

Figure 1. Modulated Polyadenylation Activity by TRAMP

(A) Polyadenylation reaction with radiolabeled (asterisk) tRNA$_i^{Met}$ (0.5 nM tRNA$_i^{Met}$, 150 nM TRAMP, 2 mM equimolar ATP-Mg^{2+}). Aliquots were removed at 1 min intervals and resolved on denaturing PAGE. Added adenosines are marked on the right.

(B) Left: contourplot of the fraction of the adenylated intermediates (A$_i$) versus reaction time for the time course in (A). The color bar shows the color progression from A$_i$ = 0 to 0.2 (contours: A$_i$ = 0.04, 0.08, 0.12, 0.16, 0.2). Right: contourplot for a simulated reaction with equal rate constants for each adenylation step (k = 1.5 min^{-1}).

(C) Quantitative analysis of individual adenylation steps. Kinetic scheme for the polyadenylation reaction. For corresponding equations and fitting of the dataset, see Experimental Procedures. Plots show representative time courses for selected species (A$_0$, A$_1$, A$_2$, A$_{10}$) from the reaction displayed in (A). Lines indicate the fit.

(D) Observed rate constants for individual adenylation steps. Points represent averages for multiple independent experiments as shown in (A). The error bars mark one standard deviation. The modulation of individual observed rate constants was independent of the order of addition of TRAMP, RNA, and ATP (Figures S1C–S1E).

(E) Rate constants at TRAMP and ATP saturation (k_{max}) for individual adenylation steps. Rate constants were determined from multiple reactions with increasing TRAMP and ATP concentrations. Error bars mark the deviation of values obtained at ATP and TRAMP saturation (Figures S1F–S1L).

(F) Apparent ATP affinity ($K_{1/2}^{ATP}$) for individual adenylation steps. Values were determined from multiple reactions with increasing ATP concentrations (Figures S1F–S1L). Error bars indicate the standard deviation.

cannot explain more intricate TRAMP functions, such as control of poly(A) tail lengths. Most likely, the yet unexplored interplay between the TRAMP components gives rise to these functions.

To examine the interplay between the TRAMP components and to illuminate the molecular basis of the poly(A) lengths control, we quantitatively analyzed individual adenylation steps by TRAMP (Trf4p, Air2p, Mtr4p) from *S. cerevisiae*. We found that TRAMP inherently limits the poly(A) tail length through modulation of individual adenylation rate constants and ATP affinities. This modulation depends on the number of 3′-terminal adenosines, a finding that corresponds to and explains the restriction of poly(A) tails on TRAMP targets in vivo (Wlotzka et al., 2011). Most intriguingly, the RNA helicase Mtr4p elicits the modulation of the polyadenylation activity of TRAMP, by detecting the number of 3′-terminal adenosines in the RNA substrate. Mtr4p impacts RNA binding, ATP affinity, and rate constants for both adenylation and TRAMP dissociation, all as a function of the number of 3′ adenylates, but without involving duplex-unwinding activity. Our findings establish Mtr4p as critical regulator of polyadenylation, an unprecedented function for an RNA helicase. Mtr4p controls the activity of the poly(A) polymerase Trf4p in an equally unprecedented fashion, through a series of energetically small but highly coordinated effects on multiple reaction parameters.

RESULTS

TRAMP Displays Modulated Polyadenylation Activity

To quantitatively characterize polyadenylation by TRAMP from *S. cerevisiae*, we reconstituted the complex from recombinant components (Figures S1A and S1B available online). Polyadenylation activity of the reconstituted TRAMP was first measured using tRNA$_i^{Met}$ (Figure 1A). This RNA resembles one of the physiological targets of TRAMP and had been previously used to detect polyadenylation activity of TRAMP obtained from yeast (Kadaba et al., 2004; Wang et al., 2008). Reactions were performed under pre-steady-state conditions (i.e., enzyme excess over the substrate) because the kinetic description of this

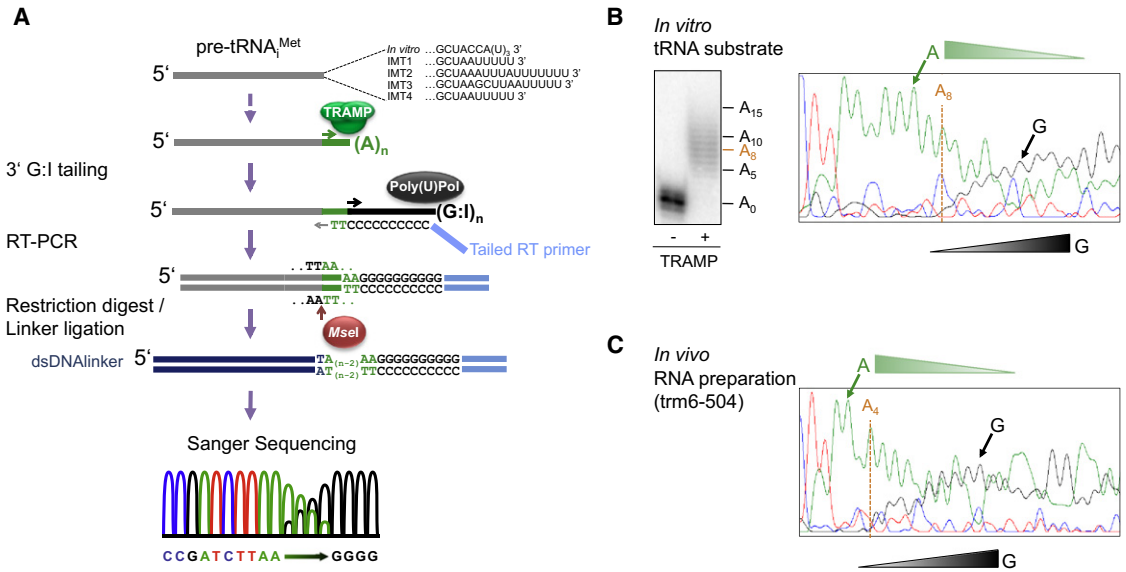

Figure 2. Accumulation of Poly(A) Tails with Approximately Four Adenosines on Hypomethylated pre-tRNA$_i^{Met}$ In Vivo

(A) Experimental scheme to measure poly(A) tail lengths of pre-tRNA$_i^{Met}$ in vivo by Sanger sequencing. The heterogeneous 3′ termini of pre-tRNA$_i^{Met}$ (*IMT1*∼*4*) are displayed.

(B) Left panel: In vitro-transcribed tRNA$_i^{Met}$ with three 3′-terminal uridines, polyadenylated by TRAMP. The number of appended adenosines is marked. Right panel: Representative Sanger sequencing chromatogram for this RNA after the poly(A) tail length measurement procedure shown in (A). The dashed line at A_8 indicates the start of the decrease in the A signal and the increase in G signal.

(C) Representative sequencing chromatogram for the cellular pre-tRNA$_i^{Met}$ sample. The dashed line at A_4 indicates the start of the decrease in A signal and the increase in G signal. Experiments were repeated multiple times and virtually identical chromatograms were obtained.

reaction regime contains fewer parameters than steady-state regimes and thus provides the most accurate quantitative data. Polyadenylation time courses were analyzed by denaturing PAGE to resolve polyadenylated species at single-nucleotide resolution (Figure 1A).

Plots of the fractions of polyadenylated species versus reaction time revealed accumulation of species with 3 to 5 adenosines in a time window from approximately 1 to 3 min (Figure 1B). Over longer reaction times, the poly(A) tail grew to 15 nt and longer. The temporary accumulation of species with 3–5 adenosines suggested a modulation of the polyadenylation activity in response to the number of added nucleotides. To test this assertion, we determined rate constants for individual adenylation steps. A simple kinetic scheme consisting of a series of irreversible, pseudo-first-order reactions faithfully described the experimental data (Figure 1C). The observed rate constants for individual adenylation steps (k_{obs}) represent multiple physical processes, including adenylation and dissociation of TRAMP from the RNA.

Plots of rate constants versus the corresponding number of added adenosines revealed a clear modulation of the polyadenylation activity. Rate constants increased for the first three steps and then decreased to fairly constant levels (Figure 1D). The resulting peak in rate constants explains the temporary accumulation of RNA species with 3–5 adenosines in a straightforward manner: TRAMP forms these species relatively fast but extends them only slowly.

To gain further insight into the molecular basis of the modulated polyadenylation activity, we examined the dependence of individual rate constants on the ATP concentration. We determined the functional affinity for ATP ($K_{1/2,ATP}$) for each adenylation step and each adenylation rate constant at ATP and TRAMP saturation (k_{max}, Figure 1E, Figures S1F–S1L). The observed peak in polyadenylation rate constants at A_3 broadened slightly at ATP saturation (Figure 1E). Most notable was a pronounced peak of low ATP affinity at A_5/A_6 (Figure 1F). This peak indicates an approximately 20-fold decrease in ATP affinity for the polyadenylation reaction at A_5/A_6, compared to earlier and later adenylation steps. This drop in ATP affinity occurs immediately after the peak for the highest adenylation rate constant at A_3, revealing that the decrease in adenylation rate constants is accompanied by a marked reduction in ATP affinity. Thus, modulation of ATP affinity and adenylation rate constants synergistically favor the temporal accumulation of species with 3–5 adenosines.

Hypomethylated Pre-tRNA$_i^{Met}$, a Prototypical TRAMP Target, Accumulates Poly(A) Tails with Approximately Four Adenosines In Vivo

We next examined whether the physiological TRAMP target, hypomethylated tRNA$_i^{Met}$ precursor (pre-tRNA$_i^{Met}$) (Kadaba et al., 2004, 2006), accumulated similarly short poly(A) tails in vivo. To measure the poly(A) tail lengths of cellular pre-tRNA$_i^{Met}$ with single-base resolution, we adopted a 3′RACE strategy (Figure 2A). We isolated total RNA from the yeast *trm6-504* strain, where the nonfunctional tRNA m^{1}A methylase Trm6p leads to accumulation of hypomethylated pre-tRNA$_i^{Met}$ that is targeted by TRAMP (Kadaba et al., 2004). Following the

extension of the RNA 3′ ends with guanosine-inosine tails, polyadenylated pre-tRNA$_i^{Met}$ were specifically amplified by RT-PCR. We accounted for the heterogeneity in the 3′ ends of pre-tRNA$_i^{Met}$ (Kadaba et al., 2004) by processing of the PCR products with the restriction enzyme MseI, which was possible because all precursors end with at least two 3′ Us (Figure 2A). The isolated pre-tRNA$_i^{Met}$ poly(A) tails were ligated to a piece of synthetic DNA, amplified and subjected to Sanger sequencing to delineate the number of added adenosines (Figure 2A).

The method was calibrated with a tRNA$_i^{Met}$ processed in vitro (gel panel in Figure 2B). The corresponding sequencing chromatogram shows excellent agreement between input and final sequencing result (Figure 2B). The robustness of the method was further tested with longer, in vitro-generated poly(A) tail lengths, and similar agreements were seen (data not shown). We then measured the lengths of poly(A) tails of pre-tRNA$_i^{Met}$ appended in vivo (Figure 2C). The corresponding Sanger chromatogram indicates accumulation of RNA species with roughly four adenosines (Figure 2C), in excellent agreement with our polyadenylation measurements in vitro (Figure 1). Accumulation of similarly short poly(A) tails on other TRAMP targets in vivo had been observed by others (Grzechnik and Kufel, 2008; Lebreton et al., 2008; Wlotzka et al., 2011). The striking correlation between the poly(A) tail length distribution of TRAMP targets in vivo and the temporary accumulation of short poly(A) tails in vitro is consistent with the notion that TRAMP displays modulated polyadenylation activity in the cell as well.

Modulated Polyadenylation Activity with Generic Model Substrates

To investigate how polyadenylation activity by TRAMP was modulated, we next examined in vitro whether the modulation was specific for physiological TRAMP targets, or if TRAMP also polyadenylated simple model RNAs in a similar fashion. First, we tested a substrate consisting of a 16 bp duplex with a single-nucleotide overhang at the 3′ end (Figure 3A). The protruding nucleotide was necessary to obtain appreciable levels of polyadenylation. On a 16 bp blunt end duplex, TRAMP displayed exceedingly low, unquantifiable activity (data not shown).

Adenylation rate constants (k_{max}) for the RNA duplex with the single-nucleotide overhang displayed a clear peak, and ATP affinities for individual adenylation steps ($K_{1/2,ATP}$) showed a pronounced peak of low ATP affinity (Figure 3A), as seen for the tRNA$_i^{Met}$ substrate (Figure 1). Although both peaks were slightly shifted, compared to the tRNA$_i^{Met}$ substrate, the sharp decrease in ATP affinity coincided again with the decrease in adenylation rate constants (Figure 3A). Extending the duplex to 23 bp had little effect on overall adenylation rate constants, presence of the characteristic peak in adenylation rate constants, and the corresponding decrease in ATP affinity, although the peaks were slightly shifted, compared to the 16 bp duplex (Figure 3B). The data obtained with these simplified model substrates clearly indicated that modulated polyadenylation activity is not restricted to physiological targets, but an inherent feature of TRAMP.

The slight shifts of the peaks for polyadenylation rate constants and ATP affinities for the different substrates suggested potential effects of RNA structure on the modulation. It had been shown that RNA structure affected Mtr4p binding (Weir et al., 2010), but it was also possible that the modulation with the tested substrates was caused by Mtr4p-mediated duplex unwinding. To test whether the modulation of polyadenylation depended on duplex unwinding, we measured polyadenylation of a single-stranded RNA (ssRNA). If modulation required unwinding, then the absence of duplexes would eliminate or drastically change the modulation. Whereas TRAMP displayed only weak, unquantifiable activity on a 17 nt ssRNA (Figures S2D and S2E), a 24 nt ssRNA was robustly adenylated (Figure 3C). Both adenylation rate constants (k_{max}) and ATP affinities for the individual adenylation steps ($K_{1/2,ATP}$) displayed the peaks indicating modulated polyadenylation (Figure 3C). Similar modulation was seen for other ssRNAs longer than 17 nt (data not shown). The modulated polyadenylation activity on single-stranded RNA indicates that the modulation is not based on duplex unwinding by TRAMP. Notwithstanding, unwinding could still contribute to a small extent to the observed slight influence of RNA secondary structure on TRAMP activity.

The Modulation of Polyadenylation Activity Depends on Mtr4p

If duplex unwinding was not causing the modulation of polyadenylation activity, did the helicase Mtr4p affect the modulation at all? To answer this question, we measured polyadenylation by a TRAMP complex without Mtr4p (Trf4p/Air2p). With the 16 bp duplex substrate described above, Trf4p/Air2p showed only low, unquantifiable levels of polyadenylation activity (Figures S3A and S3B). The 24 nt ssRNA and the 23 bp substrates were robustly polyadenylated (Figures 4A and 4B). With both substrates, Trf4p/Air2p produced longer poly(A) tails than TRAMP over comparable timeframes (Figures 4A and 4B). Adenylation rate constants increased for the first two steps but did not produce the characteristic peak seen with complete TRAMP (Figure 3). Similarly absent was the peak for ATP affinities (Figures 4A and 4B). These observations demonstrate that Trf4p/Air2p does not display the modulated polyadenylation activity seen with complete TRAMP, thus indicating a critical role of Mtr4p in the modulation. In striking correlation with our observations, Mtr4p depletion in vivo causes hyperadenylation of TRAMP targets (Houseley and Tollervey, 2006).

To illuminate how Mtr4p contributed to the modulation, we examined a TRAMP complex with a mutated Mtr4p (TRAMP$^{Mtr4\text{-}20p}$). The Mtr4-20p mutation, located in the helicase motif VI, strongly decreases unwinding and RNA-stimulated ATPase activities of Mtr4p, but TRAMP$^{Mtr4\text{-}20p}$ retains polyadenylation activity (Wang et al., 2008). With all substrates tested, TRAMP$^{Mtr4\text{-}20p}$ generated longer poly(A) tails than wild-type (WT) TRAMP at comparable reaction times (Figures 4C–4E). With the 24 nt ssRNA and the 23 bp substrates, polyadenylation rate constants and ATP affinities showed only very broad peaks, which also lacked the coordination between changes in rate constants and ATP affinity seen with WT TRAMP (Figures 4C and 4D). With the 16 bp duplex substrate, no peaks in

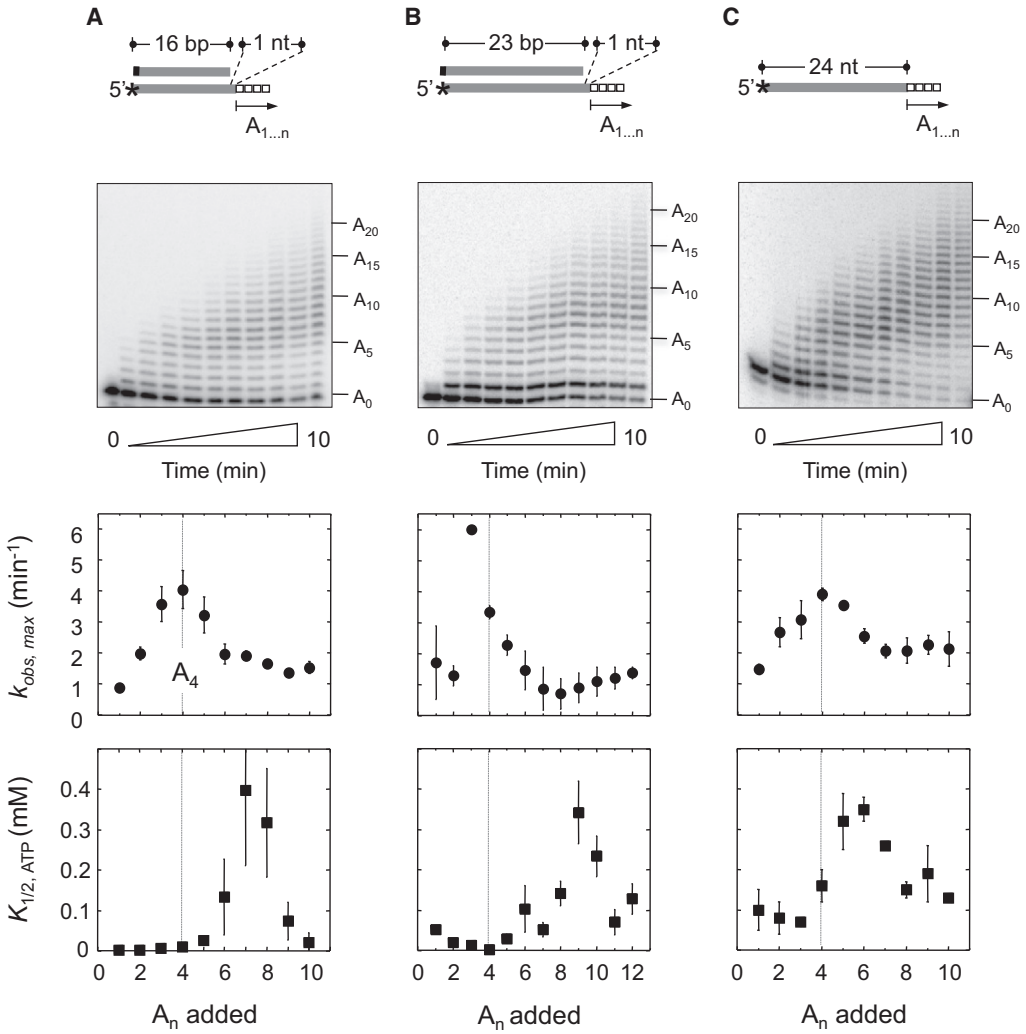

Figure 3. Modulated Polyadenylation Activity with Generic Model Substrates

(A) Polyadenylation of an RNA substrate consisting of a 16 bp duplex with 1 nt 3′-terminal overhang (100 nM TRAMP, 2 mM ATP-Mg^{2+}, and 0.5 nM RNA). The asterisk marks the radiolabel. The 16 nt top strand contained a 3′-terminal 2′,3′-dideoxy residue to prevent adenylation. Plots show rate constants at TRAMP and ATP saturation (k_{max}) and the apparent ATP affinity ($K_{1/2}^{ATP}$) for individual adenylation steps. For apparent substrate affinities ($K_{1/2}^{TRAMP}$) of individual steps, see Figure S2A. Values were determined from multiple reactions with increasing TRAMP and ATP concentrations (Figures S1F–S1L). Error bars indicate the standard deviation.

(B) Polyadenylation of a 23 bp RNA duplex with 1 nt 3′ overhang (100 nM TRAMP, 2 mM ATP-Mg^{2+}, and 0.5 nM RNA, top strand with 3′-terminal 2′,3′-dideoxy residue). Plots correspond to those in (A). Error bars indicate the standard deviation. For apparent substrate affinities, see Figure S2B.

(C) Polyadenylation of a 24 nt ssRNA substrate (100 nM TRAMP, 2 mM ATP-Mg^{2+}, and 0.5 nM RNA). Plots correspond to those in (A). Error bars indicate the standard deviation. For apparent substrate affinities, see Figure S2C.

adenylation rate constants or ATP affinities were seen (Figure 4E). These results indicate that the Mtr4-20p mutation causes a precipitous loss in the capacity of TRAMP to modulate polyadenylation activity. This observation provides further evidence that Mtr4p plays a critical role in modulating TRAMP polyadenylation activity. Moreover, the data reveal that the presence of Mtr4p in TRAMP alone is not sufficient to modulate polyadenylation. The modulation apparently requires Mtr4p with intact coordination between RNA- and ATP-binding sites, which is impaired in the Mtr4-20p mutant (Jackson et al., 2010; Wang et al., 2008; Weir et al., 2010).

The Modulation of Polyadenylation Activity Depends on the Number of 3′-Terminal Adenosines

Having implicated Mtr4p in the modulation of polyadenylation by TRAMP, we next asked how TRAMP determined at which steps to decrease adenylation rate constants and ATP affinities. A central point in this regard was whether TRAMP adjusted its activity only for adenosines that it appended or also for adenosines already present in the RNA. To distinguish between these possibilities, we measured rate constants and ATP affinities for individual adenylation steps with a 24 nt ssRNA substrate containing four 3′-terminal adenosine residues (Figure 5A). Rate

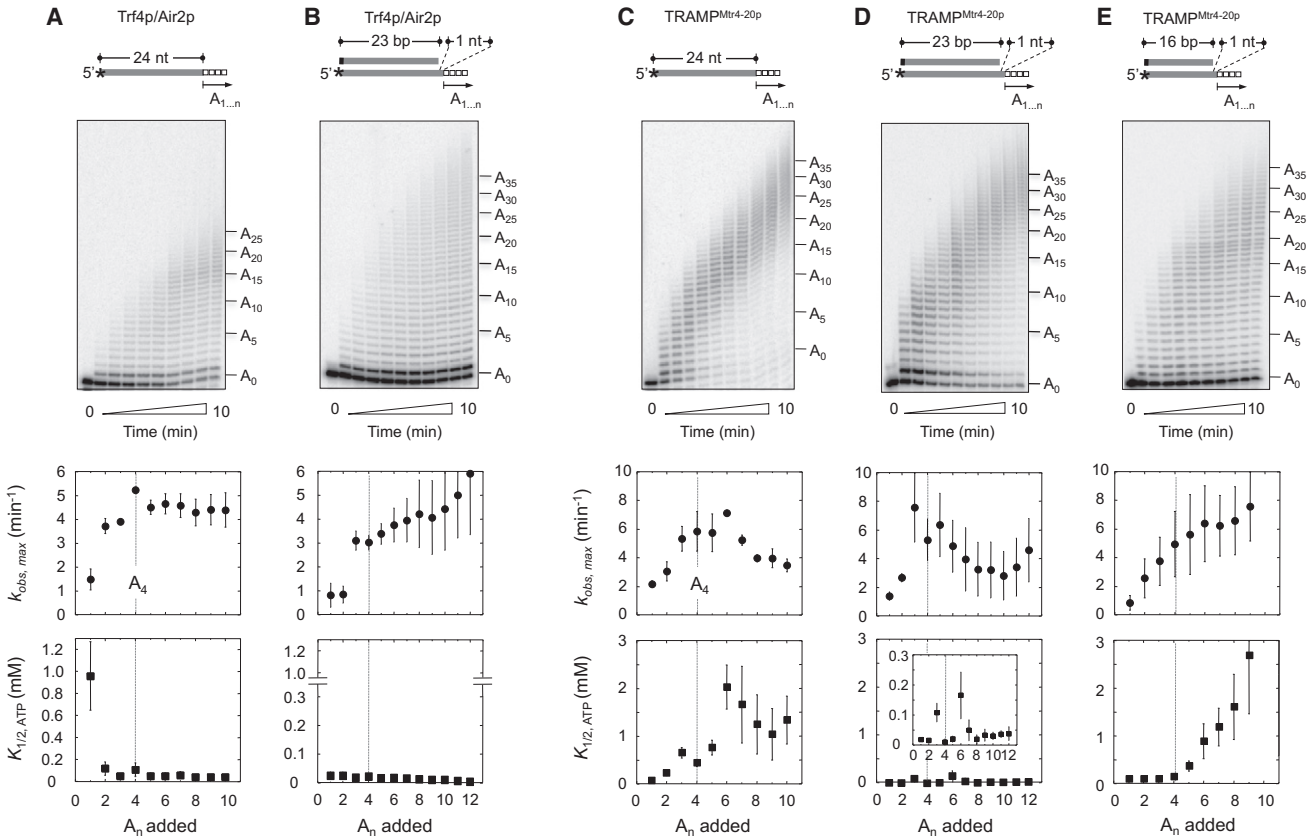

Figure 4. Removal or Mutation of Mtr4p Diminishes Modulation of Polyadenylation Activity

(A) Polyadenylation of the 24 nt ssRNA substrate (asterisk: radiolabel) with Trf4p/Air2p (100 nM Trf4p/Air2p, 2 mM ATP-Mg^{2+}, and 0.5 nM RNA). Plots correspond to those in Figure 3. For apparent substrate affinities, see Figure S3C. Values were determined from multiple reactions with increasing TRAMP and ATP concentrations (Figures S1F–S1L). Error bars indicate the standard deviation. As a reference, the dashed line marks A_4.

(B) Polyadenylation of the 23 bp RNA duplex with 1 nt 3′ overhang by Trf4p/Air2p. The y axis for the plot of apparent ATP affinities was broken to enable direct comparison of the identical reaction with WT TRAMP (Figure 3B). Error bars indicate the standard deviation. For apparent substrate affinities, see Figure S3D.

(C) Polyadenylation of the 24 nt ssRNA substrate by $TRAMP^{Mtr4\text{-}20p}$ (100 nM $TRAMP^{Mtr4\text{-}20p}$, 2 mM ATP-Mg^{2+}, and 0.5 nM RNA) (Figure S3E). Plots correspond to those in Figure 3. Error bars indicate the standard deviation. For apparent substrate affinities, see Figure S3F.

(D) Polyadenylation of the 23 bp RNA duplex (1 nt 3′ overhang) by $TRAMP^{Mtr4\text{-}20p}$. The inset shows the data with 10-fold magnification in the y axis, to enable direct comparison of the identical reaction with WT TRAMP (Figure 3C). Error bars indicate the standard deviation. For apparent substrate affinities, see Figure S3G.

(E) Polyadenylation of the 16 bp duplex (1 nt 3′-terminal overhang) by $TRAMP^{Mtr4\text{-}20p}$. Error bars indicate the standard deviation. For apparent substrate affinities see Figure S3H.

constants did not display the characteristic peak at A_4 but were remarkably similar to those measured for steps >4 for the substrate without 3′-terminal adenosines (Figure 5A). ATP affinities showed a peak shifted by four positions, compared to the substrate without the 3′-terminal adenosines (Figure 5A, lower panel). This characteristic shift was not seen with a 24 ssRNA substrate containing four consecutive adenosines within the sequence (Figure 5B). The data demonstrate that TRAMP adjusts its activity based on the presence of a critical number of 3′-terminal adenosines but irrespective of whether or not they are appended by TRAMP.

Residues outside the Helicase Domain of Mtr4p Participate in the Detection of 3′-Terminal Nucleotides

Because Mtr4p modulated polyadenylation, we next probed whether and how the 3′-terminal nucleotides were detected by Mtr4p during polyadenylation. A recent crystal structure of Mtr4p indicated a potential base recognition site, outside the helicase core (Molecule B in Weir et al., 2010) (Figures 6A and 6B). This structure suggested that E947, which is highly conserved in Mtr4p orthologs, contacts adenosine-specific groups on the fourth base from the 5′ end of the RNA bound in the structure (Figure 6C). Reasoning that E947 might be involved in the identification of the critical number of 3′-terminal adenosines, we replaced E947 with an alanine. TRAMP with Mtr4p(E947A) ($TRAMP^{Mtr4p(E947A)}$) produced longer poly(A) tails than WT TRAMP over identical reactions times (Figure 6D). The peak in adenylation rate constants seen with $TRAMP^{Mtr4p(E947A)}$ was significantly broader than with WT TRAMP. No clear peak at all was seen for ATP affinities, which also were much lower for later steps (7–10) than for WT TRAMP (Figure 6E). Thus, $TRAMP^{Mtr4p(E947A)}$ markedly diminished the modulation

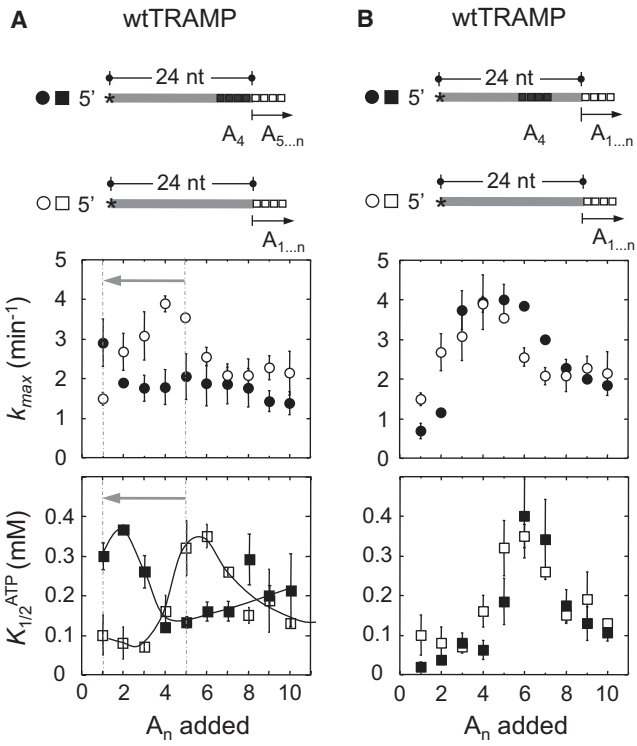

Figure 5. TRAMP Adjusts Polyadenylation Activity Based on the Number of 3′-Terminal Adenosines

(A) Polyadenylation of a 24 nt ssRNA substrate with four terminal adenosines (filled symbols) by TRAMP. For comparison, the identical substrate without the terminal adenosines is shown (open symbols, values identical to those in Figure 3C). Asterisks mark the radiolabel. Values were determined from multiple reactions with increasing TRAMP and ATP concentrations. Error bars indicate the standard deviation.

The dashed lines mark k_1 and k_5, A_1 and A_5, the arrows emphasize the shift of the peaks for adenylation rate constants and apparent ATP affinities by four nucleotides.

(B) Polyadenylation of a 24 nt ssRNA substrate with four consecutive adenosines 5 nt removed from the 3′ terminus (filled symbols). For comparison, values for the identical substrate without the terminal adenosines are shown (open symbols, panel A). Plots correspond to those in (A). Error bars indicate the standard deviation.

of polyadenylation, similar to the Mtr4-20p mutation in $TRAMP^{Mtr4\text{-}20p}$ (S4B). We conclude that E947 is important for modulating polyadenylation, consistent with a scenario where Mtr4p directly binds the 3′-terminal nucleotides, and upon detection of 3′-terminal adenosines, alters the polyadenylation activity of Trf4p.

Generation of Short Poly(A) Tails Involves Multiple Cycles of TRAMP Binding and Dissociation

To further understand how the polyadenylation activity was modulated, it was important to examine whether multiple binding and dissociation events were required until four adenosines were added. To answer this question, we determined the processivity of TRAMP for individual adenylation steps (Figure S5). The processivity is the probability of TRAMP adding the next adenosine versus dissociating from the substrate (Figure 7A). This probability is directly related to the average number of steps per binding event (Ali and Lohman, 1997) (Figure 7A).

Plots of processivity versus number of added adenosines revealed a steady increase in processivity until P = 0.64 ± 0.10 at A_4, followed by a slight decrease to P = 0.40 ± 0.03 at A_{10} (Figure 7B). For the first step, TRAMP dissociates roughly four times faster than it adds the adenosine, thus using about five binding events to add the first adenosine. For subsequent steps, dissociation and adenylation are roughly equally fast, i.e., TRAMP adds roughly two nucleotides per binding event (Figure 7B). The data show that TRAMP undergoes multiple binding and dissociation cycles to append four to five adenosines.

Mtr4p Modulates Trf4p Activity through Multiple, Energetically Small Effects

We next examined the effects of Mtr4p on TRAMP processivity. TRAMP without Mtr4p (Tr4p/Air2p) showed lower processivity than WT TRAMP for the first four steps. Subsequent steps displayed a slightly higher processivity than WT TRAMP (Figure 7C). To understand the influence of Mtr4p on a more quantitative level, we calculated forward and dissociation rate constants for each adenylation step for TRAMP with and without Mtr4p (Figures 7D and 7E). For steps 1–3, Mtr4p enhances polyadenylation rate constants, then slows these rate constants for subsequent steps (Figure 7D). In addition, Mtr4p enhances TRAMP dissociation for the first step. For subsequent steps, Mtr4p decreases dissociation rate constants, thus prolonging the time TRAMP remains bound to the RNA (Figure 7E).

To visualize the multifaceted, coordinated effects of Mtr4p on the Trf4p activity, we calculated energetic contributions of Mtr4p to adenosine addition, TRAMP dissociation, and ATP affinity for individual adenylation steps (Figures 7F and 7G). Compared to the reaction without Mtr4p, the helicase enhances adenylation rate constants and promotes tighter ATP binding for the first two steps (Figure 7H). For steps 4 and higher, Mtr4p slows adenylation rate constants and weakens ATP binding (Figure 7H). Mtr4p slows TRAMP dissociation from the RNA, except for the first step (Figure 7H). In energetic terms, the impact of Mtr4p is greatest on ATP affinities and adenylation rate constants. In general, however, Mtr4p imparts rather small changes on the individual rate constants. Yet, numerous small effects multiply over many steps and thus significantly alter the polyadenylation pattern, compared to the reaction without or with impaired Mtr4p. The coordination between changes in rate constants and changes in ATP affinity provides additional synergy to favor a temporal accumulation of short poly(A) tails (Figure 7H).

DISCUSSION

A Key Role for Mtr4p in the Regulation of Poly(A) Tail Lengths for RNAs Processed by TRAMP

In this study, we have shown that the RNA helicase Mtr4p regulates polyadenylation in the TRAMP complex. By modulating individual adenylation steps, Mtr4p facilitates a temporary accumulation of RNAs with short poly(A) tails of only three to four

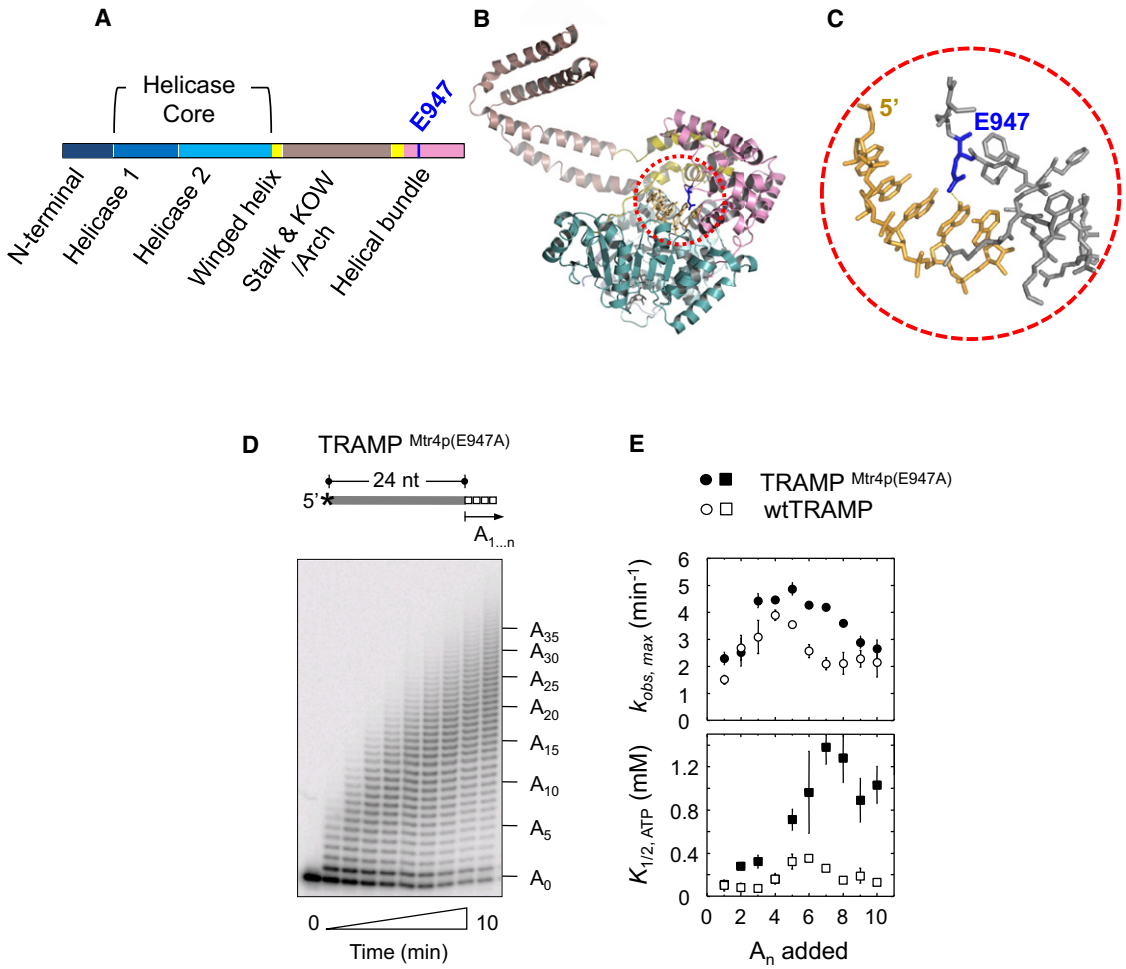

Figure 6. E947 in Mtr4p Is Critical for the Modulation of Polyadenylation

(A) Domain structure of Mtr4p (Weir et al., 2010). Domain names are shown. The blue bar represents E947.

(B) Crystal structure of Mtr4p in complex with ADP and 5 nt oligo(A). Molecule B from Weir et al. (2010) is shown. The domains are colored as in (A). E947 is shown in blue and RNA in orange. The dashed circle marks the area magnified in (C).

(C) Close up view of E947 and the 5 nt oligo(A). For clarity, only resides 945–1026 in the helical bundle domain are shown (gray). E947 is positioned to contact N6 of the 4th adenine from the 5′ end (Weir et al., 2010).

(D) Polyadenylation of the 24 nt ssRNA substrate by TRAMP$^{Mtr4p(E947A)}$ (100 nM TRAMP$^{Mtr4p(E947A)}$, 2 mM ATP-Mg^{2+}, 0.5 nM RNA).

(E) Rate constants at TRAMP$^{Mtr4p(E947A)}$ and ATP saturation ($k_{max,}$ upper panel), and apparent ATP affinity ($K_{1/2}^{ATP,}$ lower panel) for individual adenylation steps. For comparison, values for WT TRAMP are shown (open shapes). For apparent substrate affinities, see Figure S4A. Values were determined from multiple independent reactions. Error bars indicate the standard deviation.

adenosines in vitro. Strikingly, TRAMP targets in vivo accumulate similarly short poly(A) tails. We demonstrate that hypomethylated pre-tRNA$_i^{Met}$, a prototypical TRAMP target, accumulates poly(A) tails with roughly four nucleotides (Figure 2). Previous reports showed similarly short poly(A) tails on other TRAMP targets (Grzechnik and Kufel, 2008; Lebreton et al., 2008), and a recent analysis of a wide range of TRAMP targets found a distribution of poly(A) tails with a pronounced peak at four to five nucleotides (Wlotzka et al., 2011). The remarkable agreement between these observations made in vivo and our in vitro data suggests a physiological role of Mtr4p in the control of the lengths of poly(A) tails produced by TRAMP. This notion further concurs with data showing hyperadenylation upon Mtr4p depletion in vivo (Houseley and Tollervey, 2006). Removal of Mtr4p in vitro abolishes modulation and eliminates poly(A) tail length restriction (Figure 4). The striking correlation between several lines of experiments in vivo and in vitro is consistent with a pivotal, physiological role of Mtr4p in the regulation of polyadenylation by TRAMP. This role is in addition to the previously shown function of Mtr4p as exosome cofactor (Houseley and Tollervey, 2008; LaCava et al., 2005). Defects in the function as exosome cofactor might also contribute to changes in poly(A) lengths of TRAMP targets seen in vivo with functionally impaired Mtr4p.

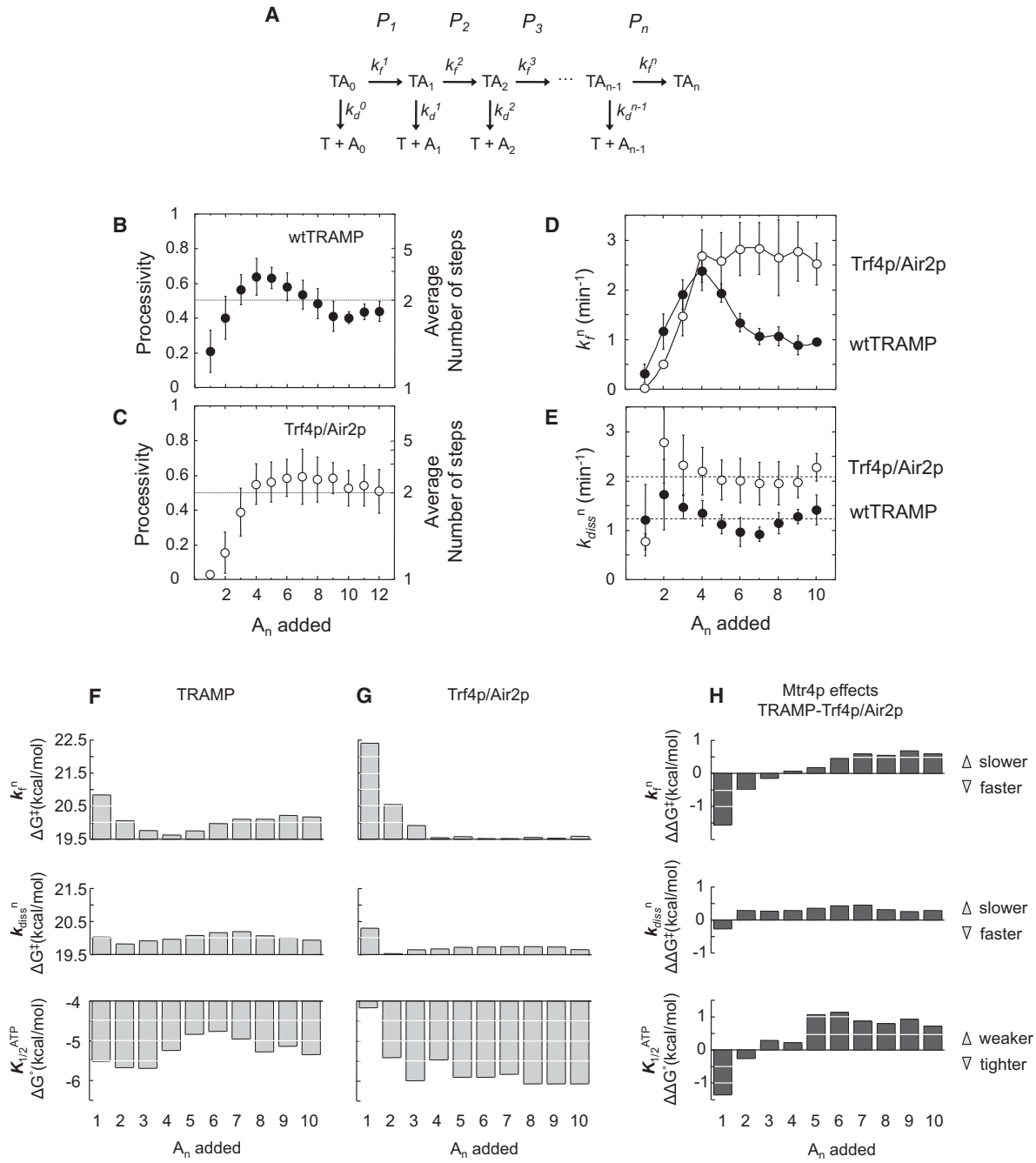

Figure 7. TRAMP Processivity and Mtr4p Effects on Multiple Reaction Parameters

(A) Reaction scheme illustrating the principle of processivity ($P_{1...n}$) for individual adenylation steps (T: TRAMP, $A_{0...n}$: adenylated RNA species, $TA_{0...n}$: TRAMP bound to the respective adenylated species, $k_f^{1...n}$: adenylation rate constant for individual step, $k_{diss}^{1...n}$: dissociation rate constant for individual step). For more experimental details, see Experimental Procedures, Extended Experimental Procedures, and Figure S5.

(B) Processivity of TRAMP for individual adenylation steps with the 24 nt ssRNA substrate. The average number of steps (N), shown at the right, corresponds to the processivity according to: $P = (N-1)/N$ (Ali and Lohman, 1997). The dotted line marks P = 0.5, N = 2. Processivity values are the average from multiple independent measurements; the error bars mark one standard deviation.

(C) Processivity of Trf4p/Air2p for individual adenylation steps of the 24 nt ssRNA substrate. Values are the average from multiple independent measurements; the error bars mark one standard deviation.

(D) Actual adenylation rate constants of TRAMP (filled circles) and Trf4p/Air2p (open circles) for individual adenylation steps with the 24 nt ssRNA substrate. Rate constants were calculated according to Equation 1 with $k_f^n + k_{diss}^n = k_{max}^n$ (Ali and Lohman, 1997). Values shown were calculated from the data in Figure 3C and Figure 4A and panels B and C. Error bars mark one corresponding standard deviation.

The multiple functional roles of Mtr4p mark this RNA helicase as central player in the control of critical steps of the TRAMP-exosome machinery. Regulation of Mtr4p could simultaneously affect multiple steps in TRAMP/exosome-mediated RNA decay and processing. The Mtr4p-mediated restriction of poly(A) tail lengths might also prevent RNAs processed by TRAMP from binding to poly(A)-binding protein (Pab1p), which requires at least 12 adenosines for stable binding in yeast (Sachs et al., 1987). In addition, the short poly(A) tails appended by TRAMP may serve as a specific signal on the RNA for subsequent processing by the exosome (Bernstein et al., 2010).

An RNA Helicase Can Control Another Enzyme in Response to Features in the RNA

Mtr4p modulates the polyadenylation activity of Trf4p for a wide range of simple model substrates (Figure 1, Figure 3, and Figure 4). These results indicate that the modulation by Mtr4p is an inherent feature of TRAMP and not conferred by certain substrates. The regulation of Trf4p by Mtr4p reveals that an RNA helicase can control another enzyme in response to features in the RNA, here the presence or emergence of a certain number of 3′ adenosines. The modulation seen with ssRNA shows that this function of Mtr4p does not depend on duplex unwinding (Figure 3). Modulation of Trf4p by Mtr4p therefore differs from unwinding-based effects of RNA helicases on viral RNA polymerases and on RNA degradation by bacterial and mitochondrial degradosomes (Borowski et al., 2010; Carpousis et al., 2009; Piccininni et al., 2002).

Notwithstanding, RNA structure slightly influences the degree by which Mtr4p modulates Trf4p (Figure 3). This effect is probably mainly caused by the impact of RNA structure on TRAMP binding, as reflected by differences in TRAMP affinities for structured versus unstructured RNAs (Figure S1 and Figure S2). Effects of RNA structure on TRAMP binding are consistent with the impact of secondary structure on RNA binding by Mtr4p, as seen previously by others (Weir et al., 2010). Nevertheless, duplex unwinding might still contribute slightly to the observed modulation of polyadenylation by Mtr4p.

Although the modulation of Trf4p by Mtr4p does not depend on duplex unwinding, helicase activity is most likely important to stimulate exosome function on structured substrates (LaCava et al., 2005; Wang et al., 2008). RNA degradation by the exosome is thought to require ssRNA much longer than the short poly(A) tails found on TRAMP targets (Bonneau et al., 2009), and Mtr4p-catalyzed duplex unwinding may be necessary to generate sufficiently long stretches of ssRNA (Anderson and Wang, 2009).

The ability of Mtr4p to modulate Trf4p activity through a series of energetically rather minor adjustments (Figure 7H) is a notable and new paradigm for a regulatory function by an RNA helicase. It is interesting to speculate about the benefits of this mode of regulation, compared to a total shutoff of polyadenylation after a set number of adenylation steps. Numerous small adjustments might provide TRAMP with flexibility to accommodate diverse substrates (Wlotzka et al., 2011), and to coordinate polyadenylation with subsequent processing steps (Callahan and Butler, 2010).

Direct Interrogation of 3′-Terminal Bases by Mtr4p

How can we physically imagine Mtr4p to exert its modulating effects in the context of TRAMP? Guided by a recent crystal structure of Mtr4p, which suggests contacts between protein and nucleobases via residues located outside the helicase core (Weir et al., 2010), we show that at least one of these residues, E947, is important for the modulation. Mutation of E947 markedly diminishes modulation by Mtr4p (Figure 6). This convergence of structural and biochemical data suggests that Mtr4p directly reads out the sequence at the 3′ terminus in the context of TRAMP, most likely by binding the 3′ terminus in a conformation similar or identical to that seen in the crystal structure (Weir et al., 2010). This notion is supported by the diminished modulation seen with the Mtr4-20p mutation (Figures 4C–4E). This mutation impairs the coupling between ATP and RNA binding and thus interferes with ATP-dependent contacts to the RNA backbone that are established by residues in the helicase core (Weir et al., 2010).

Although Mtr4p starts to modulate Trf4p as soon as a single 3′-terminal adenosine is present, the effects increase until four to five 3′-terminal adenosines are detected (Figure 7H). This observation suggests that Mtr4p binding to four to five adenosines is needed for the restriction of the poly(A) tail length. Binding of Mtr4p to four to five adenosines is consistent with the crystal structure (Weir et al., 2010). In addition, the binding site of isolated Mtr4p was recently shown to encompass approximately five nucleotides (Bernstein et al., 2010). Mtr4p was also shown to bind RNAs with adenosines tighter than other sequences (Bernstein et al., 2008, 2010). In TRAMP, this increased affinity might contribute to the Mtr4p-induced slight slowing of TRAMP dissociation from terminal adenosines (Figures 7E and 7H).

Multiple lines of structural and biochemical evidence thus coalesce around a model where Mtr4p, in the context of TRAMP, binds to the 3′ end of a substrate RNA and thereby interrogates the sequence for 3′-terminal adenosines. Probing of the nucleobases involves the helical bundle domain, wherein E947 is located. If fewer than three to four 3′-terminal adenosines are

(E) Dissociation rate constants of TRAMP (filled circles) and Trf4p/Air2p (open circles) for individual adenylation steps with the 24 nt ssRNA substrate. Rate constants were calculated with Equation S7, using the values for P^n and k_f^n determined in (B)–(D). Error bars mark one corresponding standard deviation.

(F and G) Free activation enthalpies ($\Delta G^{\ddagger}$) for adenylation (upper panels) and dissociation (middle panels), and the free energy for ATP affinities (ΔG°, lower panels) for individual adenylation steps for TRAMP (F) and Trf4p/Air2p (G), measured for the 24 nt ssRNA substrate. Free activation enthalpies were calculated according to $\Delta G^{\ddagger} = -RT \cdot \ln(hk/k_bT)$ (R: gas constant, T: temperature, h: Planck constant, k: rate constants determined in panels D and E, k_b: Boltzmann constant). Free energies for functional ATP affinities were calculated according to $\Delta G^{\circ} = -RT \cdot \ln(1/K_{1/2}^{ATP})$, using the ATP affinities ($K_{1/2}^{ATP}$) determined in Figure 3C (TRAMP) and Figure 4A (Trf4p/Air2p).

(H) Mtr4p effects on free activation enthalpies for adenylation (upper panel) and dissociation (middle panel), and on the free energies of functional ATP affinities (lower panels) for individual adenylation steps. The effect is expressed as difference in the respective free activation enthalpies and free energies shown in (F), e.g., $\Delta\Delta G^{\ddagger} = \Delta G^{\ddagger}(\text{TRAMP}) - \Delta G^{\ddagger}(\text{Trf4p/Air2p})$. The arrows on the right show how energy differences correspond to slower/faster rate constants and weaker/tighter ATP binding for each adenylation step.

detected, Mtr4p modestly stimulates Trf4p activity (Figure 7H). Upon detection of roughly four 3′-terminal adenosines, Mtr4p restricts further adenylation by TRAMP. Addition of four adenosines by TRAMP involves multiple binding and dissociation events (Figure 7B), which provide repeated opportunities for Mtr4p to interrogate the 3′-terminal bases and to adjust the Trf4p activity. Which molecular events take place during this adjustment will be a central question in the further investigation of TRAMP function.

EXPERIMENTAL PROCEDURES

Protein Expression and Purification

Recombinant TRAMP complex was generated by combining lysate of *E. coli* BL21(DE3) coexpressing Trf4p/Air2p (pETDuet-His$_6$-AIR2-TRF4-FLAG) and lysate of *E. coli* BL21(DE3) pLysS expressing Mtr4p (pET15b-His$_6$-MTR4). Clarified lysates from the two strains were combined in volumes containing a roughly 5-fold molar excess of Mtr4p over Trf4p/Air2p, followed by incubation with cobalt-sepharose (TALON metal affinity resin, Clontech). Samples were further purified with FLAG M2 affinity gel (Sigma) and eluted with FLAG peptide (Sigma). The FLAG peptide was removed from the TRAMP preparation using NAP-25 columns (GE Healthcare). Equimolar ratio of all components in the final TRAMP preparation was verified by size-exclusion chromatography and sucrose density gradient centrifugation, and integrity of the components by SDS-PAGE (Figures S1A and S1B). TRAMP concentrations were determined by Coomassie staining using BSA as standard. Aliquots were frozen in liquid nitrogen and stored at −80°C. TRAMP$^{Mtr4\text{-}20p}$, TRAMP^{E947A}, and Trf4p/Air2p were purified and stored using identical procedures. For construction of expression plasmids, see Extended Experimental Procedures.

RNA Substrates

S. cerevisiae tRNA$_i^{Met}$ was transcribed in vitro using T7 RNA polymerase (Senger et al., 1992) and purified with denaturing PAGE. All other RNAs were synthetic oligonucleotides purchased from Dharmacon. For sequences see Extended Experimental Procedures. All RNAs were 5′-radiolabeled with P^{32} using T4 polynucleotide kinase (PNK, NEB) and purified with denaturing PAGE. Duplex substrates were generated and purified as described (Yang and Jankowsky, 2005).

Polyadenylation Reactions

Polyadenylation reactions were performed at 30°C in a temperature-controlled heating block in a buffer containing 40 mM MOPS (pH 6.5), 100 mM NaCl, 0.5 mM $MgCl_2$, 5% glycerol, 0.01% Nonidet P-40, 2 mM DTT, 0.7 U/μl Protector RNase Inhibitor (Roche). Prior to the reaction, radiolabeled RNA (0.5 nM final concentration) was incubated for 5 min with the indicated concentration of TRAMP. Reactions were started by addition of equimolar ATP and $MgCl_2$ at the concentrations indicated. The order of addition of TRAMP, RNA, and ATP-$MgCl_2$ did not affect the observed modulation of the polyadenylation activity (Figures S1C–S1E). Aliquots were removed at times indicated, and the reaction was stopped by addition of an equal volume of 80% formamide and dye markers. Samples were applied to denaturing PAGE and run to single-nucleotide resolution. Gels were dried, and individual bands were visualized on a Storm PhosphorImager (GE Healthcare) and quantified using the ImageQuant software (GE Healthcare).

Calculation of Individual Adenylation Rate Constants

Individual adenylation rate constants at a given ATP concentration were determined by describing the polyadenylation reaction as a series of irreversible 1st order reactions:

$$A_0 \xrightarrow{k_1} A_1 \xrightarrow{k_2} A_2 \xrightarrow{k_3} \ldots A_{n-1} \xrightarrow{k_n} A_n \ldots \qquad \text{(Scheme 1)}$$

(A_0: RNA substrate, $A_{1\ldots n}$: species with 1…n adenosines, $k_{1\ldots n}$: pseudo-first order rate constants for individual adenylation steps). Derivation of explicit kinetic descriptions of time courses for all individual adenylated species (described in Extended Experimental Procedures) yielded:

$$\begin{cases} A_0(t) = e^{-k_1 t} \\ A_i(t) = \prod_{j=1}^{i} k_j \sum_{j=1}^{i+1} \dfrac{e^{-k_j t}}{\prod_{p=1,\, p\neq j}^{i+1} (k_p - k_j)} \end{cases} \mathrm{i} = 1\ldots\mathrm{n}, \qquad \text{(Equations 1)}$$

If all steps have identical rate constants ($k_i = k_u$ (i = 1…n)), Equations 1 adopt the form published by Lucius et al. (2003). To calculate rate constants from the measured time courses, we implemented Equations 1 in a computer routine using *Mathematica* 6 (Wolfram Research). Calculated rate constants were verified by simulating time courses with the determined values.

Measurement of Poly(A) Tail Length of Hypomethylated Pre-tRNA$_i^{Met}$ In Vivo

Total RNA was prepared from the *trm6-504* strain, and G:I tails were appended with poly(U) polymerase (NEB). Reverse transcription primer was added and first-strand synthesis was performed with MMLV-RT (NEB). Obtained cDNA were amplified with *Taq* polymerase (Roche) and tRNA$_i^{Met}$-specific primers. Specific amplification of pre-tRNA$_i^{Met}$ was verified by Sanger sequencing (data not shown). To account for the heterogeneity of pre-tRNA$_i^{Met}$ 3′ ends, the RT-PCR products were digested with MseI (NEB), which removed the tRNA moiety from the 3′G-tailed poly(A) tails of the pre-tRNA$_i^{Met}$ (Figure 2). A dsDNA linker was then ligated to the separated poly(A) tails, and ligated products were amplified with Herculase polymerase (Stratagene). PCR products were purified and sequenced by ACGT Inc. (Wheeling, IL, USA).

The procedure was calibrated using in vitro-transcribed tRNA$_i^{Met}$. Several 3′-terminal Us were appended to the RNA using TRAMP and UTP instead of ATP. The species containing three 3′-terminal U was isolated on denaturing PAGE and then polyadenylated with TRAMP. The reaction was analyzed on denaturing PAGE to visualize the poly(A) tail distribution (Figure 2B). The purified RNA was subjected to the procedure outlined above for the total RNA from the *trm6-504* strain, thus allowing a direct correlation between in vitro data and the poly(A) tail length analysis by Sanger sequencing (for more detailed protocols see Extended Experimental Procedures).

Determination of Processivity for Individual Adenylation Steps

To determine the processivity for individual adenylation steps, polyadenylation reactions were performed as described above using 0.5 nM of 24 nt single-stranded substrate and 150 nM WT TRAMP or Trf4p/Air2p. However, at defined times after the reaction start (t_1), 10 μM of a scavenger RNA (73 nt RNA of unrelated sequence) was added to prevent rebinding of TRAMP to the substrate (Figure S5). Control reactions confirmed complete prevention of TRAMP rebinding (data not shown). After scavenger addition, aliquots were removed from the reaction at defined times. Samples were applied to a 15% denaturing polyacrylamide gel and run to single-nucleotide resolution as described above. Gels were dried, and individual bands were visualized on a Storm PhosphorImager and quantified using the ImageQuant software. Distributions of all polyadenylated species at a given time (t_1) before and after scavenger addition (when this distribution no longer changed, $t_2 \sim 10$ min after scavenger addition, Figure S5) were determined, and processivity was calculated according to:

$$\begin{cases} P_1 = 1 - \dfrac{A_0(t_1 + t_2)}{A_0(t_1)} \\ P_{i+1} = 1 - \dfrac{A_i(t_1 + t_2)}{A_i(t_1) + \sum_{j=0}^{i-1} \left(A_j(t_1) \prod_{p=j+1}^{i} P_p \right)} \end{cases} \mathrm{i} = 1\ldots\mathrm{n}, \qquad \text{(Equations 2)}$$

To calculate processivities from the measured distributions, the equations were implemented into a computer routine using the *Mathematica* 6 platform. Derivation of Equations 2, more detailed descriptions of the experimental steps, and representative data are described in the Extended Experimental Procedures.

SUPPLEMENTAL INFORMATION

Supplemental Information includes Extended Experimental Procedures and five figures and can be found with this article online at doi:10.1016/j.cell.2011.05.010.

ACKNOWLEDGMENTS

We thank the members of the Jankowsky and Anderson labs and Dr. Mike Harris (Case Western) for helpful discussions and Drs. Timothy Nilsen and Pat Maroney (Case Western) for advice on the determination of the poly(A) tail length of pre-tRNA$_i^{Met}$ in vivo. This work was supported by grants from the NIH to E.J. (GM067700) and J.T.A. (GM069949).

Received: August 5, 2010
Revised: March 3, 2011
Accepted: May 6, 2011
Published: June 9, 2011

REFERENCES

Ali, J.A., and Lohman, T.M. (1997). Kinetic measurement of the step size of DNA unwinding by Escherichia coli UvrD helicase. Science *275*, 377–380.

Anderson, J.T., and Wang, X. (2009). Nuclear RNA surveillance: no sign of substrates tailing off. Crit. Rev. Biochem. Mol. Biol. *44*, 16–24.

Bernstein, J., Patterson, D.N., Wilson, G.M., and Toth, E.A. (2008). Characterization of the essential activities of Saccharomyces cerevisiae Mtr4p, a 3′->5′ helicase partner of the nuclear exosome. J. Biol. Chem. *283*, 4930–4942.

Bernstein, J., Ballin, J.D., Patterson, D.N., Wilson, G.M., and Toth, E.A. (2010). Unique properties of the Mtr4p-poly(A) complex suggest a role in substrate targeting. Biochemistry *49*, 10357–10370.

Bonneau, F., Basquin, J., Ebert, J., Lorentzen, E., and Conti, E. (2009). The yeast exosome functions as a macromolecular cage to channel RNA substrates for degradation. Cell *139*, 547–559.

Borowski, L.S., Szczesny, R.J., Brzezniak, L.K., and Stepien, P.P. (2010). RNA turnover in human mitochondria: more questions than answers? Biochim. Biophys. Acta *1797*, 1066–1070.

Callahan, K.P., and Butler, J.S. (2010). TRAMP complex enhances RNA degradation by the nuclear exosome component Rrp6. J. Biol. Chem. *285*, 3540–3547.

Carpousis, A.J., Luisi, B.F., and McDowall, K.J. (2009). Endonucleolytic initiation of mRNA decay in Escherichia coli. Prog. Mol. Biol. Transl. Sci. *85*, 91–135.

de la Cruz, J., Kressler, D., Tollervey, D., and Linder, P. (1998). Dob1p (Mtr4p) is a putative ATP-dependent RNA helicase required for the 3′ end formation of 5.8S rRNA in Saccharomyces cerevisiae. EMBO J. *17*, 1128–1140.

Egecioglu, D.E., Henras, A.K., and Chanfreau, G.F. (2006). Contributions of Trf4p- and Trf5p-dependent polyadenylation to the processing and degradative functions of the yeast nuclear exosome. RNA *12*, 26–32.

Grzechnik, P., and Kufel, J. (2008). Polyadenylation linked to transcription termination directs the processing of snoRNA precursors in yeast. Mol. Cell *32*, 247–258.

Houseley, J., and Tollervey, D. (2006). Yeast Trf5p is a nuclear poly(A) polymerase. EMBO Rep. *7*, 205–211.

Houseley, J., and Tollervey, D. (2008). The nuclear RNA surveillance machinery: the link between ncRNAs and genome structure in budding yeast? Biochim. Biophys. Acta *1779*, 239–246.

Houseley, J., and Tollervey, D. (2009). The many pathways of RNA degradation. Cell *136*, 763–776.

Jackson, R.N., Klauer, A.A., Hintze, B.J., Robinson, H., van Hoof, A., and Johnson, S.J. (2010). The crystal structure of Mtr4 reveals a novel arch domain required for rRNA processing. EMBO J. *29*, 2205–2216.

Jensen, T.H., and Moore, C. (2005). Reviving the exosome. Cell *121*, 660–662.

Kadaba, S., Krueger, A., Trice, T., Krecic, A.M., Hinnebusch, A.G., and Anderson, J. (2004). Nuclear surveillance and degradation of hypomodified initiator tRNAMet in S. cerevisiae. Genes Dev. *18*, 1227–1240.

Kadaba, S., Wang, X., and Anderson, J.T. (2006). Nuclear RNA surveillance in Saccharomyces cerevisiae: Trf4p-dependent polyadenylation of nascent hypomethylated tRNA and an aberrant form of 5S rRNA. RNA *12*, 508–521.

Keller, W. (1995). No end yet to messenger RNA 3′ processing!. Cell *81*, 829–832.

LaCava, J., Houseley, J., Saveanu, C., Petfalski, E., Thompson, E., Jacquier, A., and Tollervey, D. (2005). RNA degradation by the exosome is promoted by a nuclear polyadenylation complex. Cell *121*, 713–724.

Lebreton, A., Tomecki, R., Dziembowski, A., and Séraphin, B. (2008). Endonucleolytic RNA cleavage by a eukaryotic exosome. Nature *456*, 993–996.

Liu, Q., Greimann, J.C., and Lima, C.D. (2006). Reconstitution, activities, and structure of the eukaryotic RNA exosome. Cell *127*, 1223–1237.

Lucius, A.L., Maluf, N.K., Fischer, C.J., and Lohman, T.M. (2003). General methods for analysis of sequential "n-step" kinetic mechanisms: application to single turnover kinetics of helicase-catalyzed DNA unwinding. Biophys. J. *85*, 2224–2239.

Lykke-Andersen, S., Brodersen, D.E., and Jensen, T.H. (2009). Origins and activities of the eukaryotic exosome. J. Cell Sci. *122*, 1487–1494.

Piccininni, S., Varaklioti, A., Nardelli, M., Dave, B., Raney, K.D., and McCarthy, J.E. (2002). Modulation of the hepatitis C virus RNA-dependent RNA polymerase activity by the non-structural (NS) 3 helicase and the NS4B membrane protein. J. Biol. Chem. *277*, 45670–45679.

Sachs, A.B., Davis, R.W., and Kornberg, R.D. (1987). A single domain of yeast poly(A)-binding protein is necessary and sufficient for RNA binding and cell viability. Mol. Cell. Biol. *7*, 3268–3276.

San Paolo, S., Vanacova, S., Schenk, L., Scherrer, T., Blank, D., Keller, W., and Gerber, A.P. (2009). Distinct roles of non-canonical poly(A) polymerases in RNA metabolism. PLoS Genet. *5*, e1000555.

Scorilas, A. (2002). Polyadenylate polymerase (PAP) and 3′ end pre-mRNA processing: function, assays, and association with disease. Crit. Rev. Clin. Lab. Sci. *39*, 193–224.

Senger, B., Despons, L., Walter, P., and Fasiolo, F. (1992). The anticodon triplet is not sufficient to confer methionine acceptance to a transfer RNA. Proc. Natl. Acad. Sci. USA *89*, 10768–10771.

Vanácová, S., Wolf, J., Martin, G., Blank, D., Dettwiler, S., Friedlein, A., Langen, H., Keith, G., and Keller, W. (2005). A new yeast poly(A) polymerase complex involved in RNA quality control. PLoS Biol. *3*, e189.

Wang, X., Jia, H., Jankowsky, E., and Anderson, J.T. (2008). Degradation of hypomodified tRNA(iMet) in vivo involves RNA-dependent ATPase activity of the DExH helicase Mtr4p. RNA *14*, 107–116.

Weir, J.R., Bonneau, F., Hentschel, J., and Conti, E. (2010). Structural analysis reveals the characteristic features of Mtr4, a DExH helicase involved in nuclear RNA processing and surveillance. Proc. Natl. Acad. Sci. USA *107*, 12139–12144.

Wilusz, J.E., and Spector, D.L. (2010). An unexpected ending: noncanonical 3′ end processing mechanisms. RNA *16*, 259–266.

Wlotzka, W., Kudla, G., Granneman, S., and Tollervey, D. (2011). The nuclear RNA polymerase II surveillance system targets polymerase III transcripts. EMBO J. *30*, 1790–1803.

Wyers, F., Rougemaille, M., Badis, G., Rousselle, J.C., Dufour, M.E., Boulay, J., Régnault, B., Devaux, F., Namane, A., Séraphin, B., et al. (2005). Cryptic pol II transcripts are degraded by a nuclear quality control pathway involving a new poly(A) polymerase. Cell *121*, 725–737.

Yang, Q., and Jankowsky, E. (2005). ATP- and ADP-dependent modulation of RNA unwinding and strand annealing activities by the DEAD-box protein DED1. Biochemistry *44*, 13591–13601.